J Mater Sci (2008) 43:6132–6138
DOI 10.1007/s10853-008-2921-6

Structures, thermal stability, and crystalline properties of polyamide6/organic-modified Fe-montmorillonite composite nanofibers by electrospinning

Yibing Cai · Qi Li · Qufu Wei · Yibang Wu · Lei Song · Yuan Hu

Received: 11 May 2008 / Accepted: 31 July 2008 / Published online: 4 September 2008

Abstract In the present work, Fe-montmorillonite (Fe-MMT) was synthesized by hydrothermal method, and then was modified by cetyltrimethyl ammonium bromide (CTAB). The polyamide6 (PA6)/organic-modified Fe-montmorillonite (Fe-OMT) composite nanofibers were prepared by facile compounding and electrospinning. Fe-OMT was first dispersed in N, N-dimethyl formamide and then compounded with PA6 which was dissolved in formic acid. The composite solutions were electrospun to form PA6/Fe-OMT composite nanofibers. The structure, morphology, thermal stability, and crystalline properties of the composite nanofibers were characterized by Fourier transfer infrared (FTIR) spectra, Energy dispersive X-ray spectroscopy (EDX), X-ray diffraction (XRD), High-resolution electron microscopy (HREM), Scanning electron microscopy (SEM), and Thermogravimetric analyses (TGA), respectively. It was found that the silicate clay layers were well exfoliated within the composite nanofibers and were oriented along the fiber axis. The SEM images indicated that the loading of Fe-OMT decreased the diameters of composite nanofibers. TGA analyses revealed that the thermal stability was notably improved in the presence of silicate clay. It was also observed from wide-angle XRD analyses that the presence of nanoclays improved the γ-form crystals and induced the formations of α-form crystals of the PA6, attributed to effective nucleating effects of silicate clay platelets.

Y. Cai · Q. Li · Q. Wei (✉) · Y. Wu
Key Laboratory of Eco-Textiles, Ministry of Education, Jiangnan University, Wuxi 214122, Jiangsu, People's Republic of China
e-mail: qfwei@jiangnan.edu.cn

Y. Cai · L. Song · Y. Hu
State Key Laboratory of Fire Science, University of Science and Technology of China, Hefei 230027, Anhui, People's Republic of China
e-mail: yibingcai@ustc.edu

Introduction

Polyamide6 (PA6), due to its excellent physical properties, e.g., high fatigue strength, low coefficient of friction, enhanced toughness, and high resistance to a wide spectrum of fuels, oils, and chemicals, is a commercially important semicrystalline polymer [1, 2]. The recent interest in polymer/nanofiller composites, so-called polymer nanocomposites, stems from the dramatic improvement in physical properties that can be produced by just adding a small fraction of clay to a polymer matrix. It has been shown that most of the properties are enhanced in the presence of a small amount of clay. For instance, the incorporation of a few percent of clay in many cases increases the modulus, strength, gas barrier properties, thermal stability, and fire retardant properties, compared to the pure polymers or conventional microcomposites [3, 4]. The most frequently used clay is montmorillonite, MMT, which is an aluminous silicate mineral with sodium ions present between the clay layers. It is a naturally occurring 2:1 phyllosilicate. The structure consists of two fused silica tetrahedral sheets sandwiching an edge-shared octahedral sheet of either aluminium or magnesium hydroxide. The MMT crystal lattice is about 1 nm thick and with a lamellar aspect ratio of between 100 and 1,000. There have been many reports about the preparation of polymer/clay composite nanofibers by electrospinning [2, 5–11]. Most of the compounding processes have concentrated on the melting-extrusion techniques for making the polymer/clay

nanocomposites, and then preparing the composite nanofibers by electrospinning through dissolving the polymer/clay nanocomposites in solvent [2, 5–7]. Electrospinning provides not only a homogeneous dispersion within the fibers of MMT, but also yields a drastic decrease in the fiber diameter down to several tens of nanometers.

The phenomenon of isomorphous replacement in montmorillonite is very common. The Si^{4+} in the tetrahedral crystal lattice of structural level is replaced by Al^{3+}. The Al^{3+} in the octahedral lattice is replaced by Fe^{3+}, Fe^{2+}, Mg^{2+}, Cr^{3+}, Zn^{2+}, Li^{+}, etc. Due to exchange of unequal values, the electric neutrality of the structure is destroyed and some excess electrons may appear. These electrons are compensated by alkali metal cations or alkali earth metal cations, and the cations of compensation come into spaces between structure levels and distribute into the edges of lattices. Those cations are often replaced by other cations, so the clay performs some sort of distinctive functions. These types of MMT may possess different performances from natural MMT. For example, the catalysis effect of Cu^{2+}-exchanged and Fe^{3+}-exchanged montmorillonite (Cu^{2+}-MMT, Fe^{3+}-MMT) increases remarkably the charred residue of nylon6 nanocomposites [12].

From on the above literature summary, it can be found that the polymer/clay composite nanofibers were usually prepared by the melt-mixing and then electrospinning. In addition, there were few reports about the thermal stability and flammability properties of the composite nanofibers [8]. In the present work, a facile composite technique was reported. First, Fe-montmorillonite (Fe-MMT) was hydrothermally synthesized [13, 14] and then was modified by cetyltrimethyl ammonium bromide (CTAB). The difference was that Fe(III) ion replaced Al (III) ion in the crystal lattice of the MMT. Then, organic-modified Fe-montmorillonite (Fe-OMT) was dispersed in the N, N-dimethyl formamide and then compounded with PA6 which was dissolved in formic acid. The composite solution was electrospun to form PA6/Fe-OMT composite nanofibers. The structure and morphology of composite nanofibers were characterized by FTIR, EDX, XRD, HREM, and SEM. The thermal stability and crystalline properties of composite nanofibers were measured by TGA and Wide-angle XRD.

Experimental

Materials

The Polyamide6 (PA6, 1003NW8, with weight-average molecular weight 18,000, characteristic viscosity was 2.8) was supplied as pellets by UBE Industries, Japan. The used chemicals including acidic sodium silicate ($Na_2SiO_3 \cdot 9H_2O$), iron(III) chloride ($FeCl_3 \cdot 6H_2O$), zinc acetate [$Zn(CH_3COO)_2 \cdot 2H_2O$], and sodium hydroxide (NaOH) were obtained from the Shanghai Chemical Regents Company. The 99.5% N, N-dimethyl formamide (DMF), 88% formic acid, and cetyltrimethyl ammonium bromide (CTAB) were all used as received. All chemicals were of analytical grade and were used as received without further purification.

Synthesis of Fe-OMT

Fe-MMT was first synthesized using the following method. The hydrous oxide was prepared by mixing $Na_2SiO_3 \cdot 9H_2O$ with $FeCl_3 \cdot 6H_2O$ and $Zn(CH_3COO)_2 \cdot 2H_2O$ solutions to set the atomic ratio at Si/Fe/Zn = 4:1.7:0.3. The PH value of the solution was adjusted with NaOH solution and was controlled in the range of 12–12.4. Then, the slurry was sealed in a Teflon container and hydrothermally treated at 140 °C for 24 h, for obtaining Fe-MMT as a transparent yellowish brown gel without impurities. The cation exchange capacity (CEC) of the obtained Fe-MMT was 102 mequiv/100 g. The detailed method of synthesis was also reported in the literature [14].

Fe-MMT was dispersed in water and formed a suspension by vigorous stirring. Then the solution of CTAB was added to the suspension and stirred for 3 h at 80 °C. The suspension was centrifuged and washed with boiling distilled water to remove the excess CTAB, until the supernatant liquid was tested by a 0.1 mol/L $AgNO_3$ solution without yielding sedimentation. The product was then dried in vacuum and ground into powder to get the Fe-OMT.

Preparation of electrospun composite nanofibers

The slurry was prepared by dispersing Fe-OMT (0.6960 g) powder into DMF (20.00 mL) solvent using magnetic stirring for 30 min until the powder uniformly dispersed in the DMF solvent, and then sonicated for 1.5 h. Also 15 wt.% of PA6 dissolved in formic acid was prepared. The prepared clay slurry was then put into the PA6 solution, which was mixed by magnetic stirring for 30 min and then was sonicated for another 20 min. The polymer solutions were electrospun at a positive voltage of 14 kV with a working distance of 10 cm (the distance between the needle tip and the collection plate), and an ejection rate of 0.5 mL/h. The mass ratio of Fe-OMT to PA6 was 2 and 4 wt.%, and was referred to as PA6/Fe-OMT2 and PA6/Fe-OMT4 composite nanofibers, respectively.

Characterization

The Fourier transfer infrared (FTIR) spectra were recorded on a Nicolet MAGNA-IR 750 spectrometer by the standard KBr disk method in the range of 350–4,000 cm^{-1} with a resolution of 4 cm^{-1}.

X-ray diffraction (XRD) patterns were performed on the 1-mm-thick films using a Japanese Rigaku D/Max-Ra rotating anode X-ray diffractometer equipped with a Cu-Kα tube and Ni filter ($\lambda = 0.1542$ nm). Scans were run in the low angle region of $2\theta < 10^{o}$ to study the nanofiller dispersion, and in the high angle region $10^{o} < 2\theta < 40^{o}$ to follow the crystal form changes in the presence of nanoclays. To investigate the dispersion of the clay layers within the composite nanofibers, the PA6/Fe-OMT nanofibers were directly electrospun onto a 200-mesh Cu grid and observed by High-resolution electron microscopy (HREM, JEOL 2010) with an accelerating voltage of 200 kV.

Scanning electron microscope (SEM) Quanta 200 was used to examine the structures of the composite nanofibers. The samples were coated with a thin layer of gold by sputtering before the SEM imaging. Energy dispersive X-ray spectroscopy (EDX) equipped by SEM Quanta 200 was used to examine the chemical compositions of the PA6/Fe-OMT composite nanofibers. An accelerating voltage of 20 kV with accounting time of 100 s was applied.

Thermogravimetric analyses (TGA) were carried out using a TGA50H thermo-analyzer instrument from 25 to 700 °C using a linear heating rate of 10 °C/min under nitrogen flow. The nitrogen flow was 25 mL/min. Samples were measured in a sealed alumina pan with a mass of about 10 mg. The temperature and mass reproducibility of the instrument were ±2.0 °C and ±2.0%, respectively.

Results and discussion

Structures of the composites nanofibers

The FTIR spectra of Fe-OMT, PA6 nanofiber, and PA6/Fe-OMT composite nanofiber are shown in Fig. 1. It was clearly observed that the absorption peaks of O–H stretching vibration were located at 3,635 cm^{-1}, while the wide absorption peaks at about 3,300 cm^{-1} were O–H stretching vibration that formed hydrogen bonds. The characteristic bands at 1,032, 471, and 460 cm^{-1} corresponded to the stretching vibration of Si–O–Si, the stretching vibration of Fe–O, and the Si–O bending vibration of MMT, respectively. The absorption peaks at about 2,920−2,850 cm^{-1} were assigned to the C–H stretching vibration of CTAB. The characteristic absorbance bands of PA6 nanofiber occurred in the following assignments: N–H stretching vibration (3,400 cm^{-1}), CH_2 non-symmetric stretching vibration (2,920 cm^{-1}) and CH_2 symmetric stretching vibration (2,855 cm^{-1}), amide I band (1,640 cm^{-1}), and CH_2 deformation vibration (1,460 cm^{-1}), as presented in Fig. 1. It can be found from Fig. 1 that the spectra of the PA6/Fe-OMT composite nanofibers contained the characteristic bands of the Fe-OMT and PA6. The results confirmed the presence of Fe-OMT in the PA6 composite nanofibers [15].

Figure 2 indicates the EDX patterns of the PA6 nanofiber and PA6/Fe-OMT composite nanofiber. It can be seen that the PA6 nanofibers dominantly consisted of C, O, and N, as illustrated in Fig. 2a. Compared to the PA6 nanofibers, the significant amount of Fe, Zn, and Si within the PA6/Fe-OMT composite nanofibers can also be seen in Fig. 2b. This was attributed to Fe-OMT embedded in the nanofiber. The results further confirmed the presence of Fe-OMT in the PA6 composite nanofibers.

The XRD patterns of Fe-OMT and PA6/Fe-OMT composite nanofibers are presented in Fig. 3. The maximum

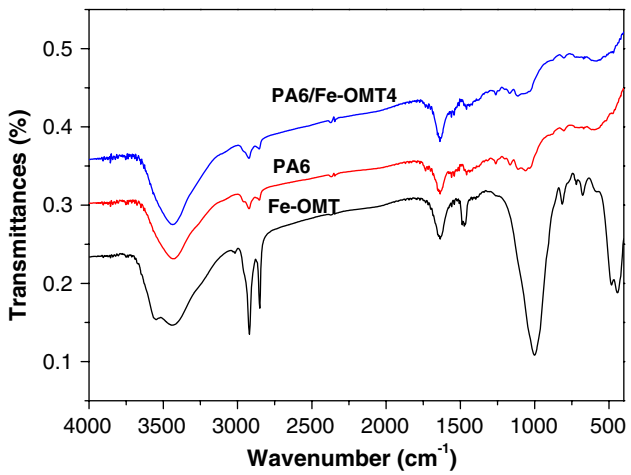

Fig. 1 FTIR spectra of the Fe-OMT, electrospun PA6 nanofiber, and PA6/Fe-OMT4 composite nanofiber

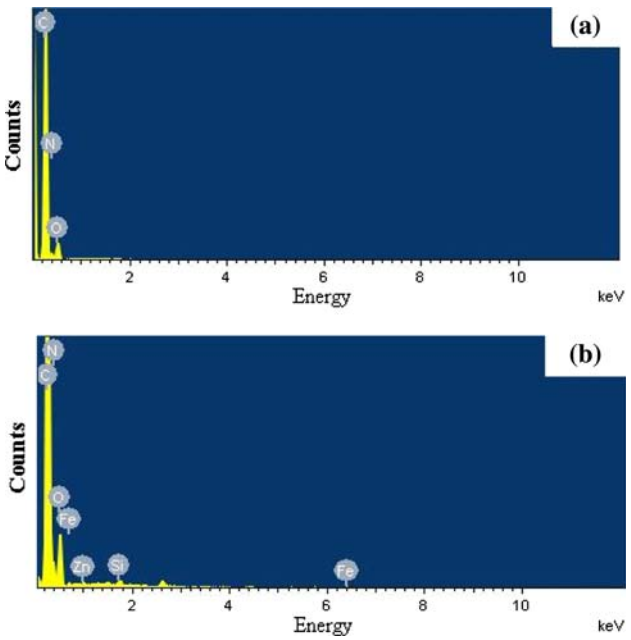

Fig. 2 EDX spectra of (**a**) PA6 nanofiber and (**b**) PA6/Fe-OMT4 composite nanofiber

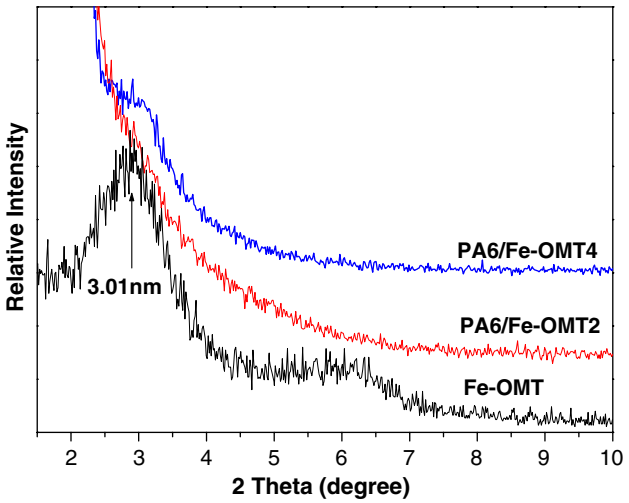

Fig. 3 XRD patterns of Fe-OMT and PA6/Fe-OMT composite nanofibers

peaks corresponded to the (001) plane reflection of the silicate clays. The XRD patterns indicated that the d_{001} peak of Fe-OMT with the corresponding interlayer spacing of 3.01 nm was observed at lower angle ($2\theta = 2.9°$). There were no observable diffraction peaks for PA6 composite nanofibers loaded with 2 wt.% Fe-OMT, as indicated in Fig. 3. This observation revealed that most of Fe-OMT was exfoliated and well dispersed in the PA6 composite nanofibers. However, a broad diffraction peak for the PA6 composite nanofibers occurred when the amount of Fe-OMT increased to 4 wt.%. The reason may be that the higher loading of Fe-OMT was propitious to form an intercalated-delaminated structure.

To further confirm the dispersion of silicate clay platelets in the PA6 composite nanofibers, HREM investigations were required. The HREM image in Fig. 4 reveals the nano-size silicate clay platelets in the electrospun PA6 composite nanofiber. It can be clearly observed that silicate clay platelets were well dispersed and exfoliated with some larger intercalated tactoids (multiplayers) in the composite nanofibers. The HREM images also clearly indicated that the silicate clay layers were almost oriented in the fiber axial direction, as shown in Fig. 4. This was due to the higher draw ration that imparted a larger stress on the fiber as it was being formed during the electrospinning process and gave rise to a proper alignment of the 2-dimensional nanoclays along the fiber axis. Meanwhile, the orientation also confirmed that extensional forces were exerted on the composite nanofibers during electrospinning.

Morphology of composite nanofibers

The SEM images of electrospun PA6 nanofiber and PA6/Fe-OMT composite nanofiber, collected on the aluminum foil, are illustrated in Fig. 5. The nanofibers were randomly

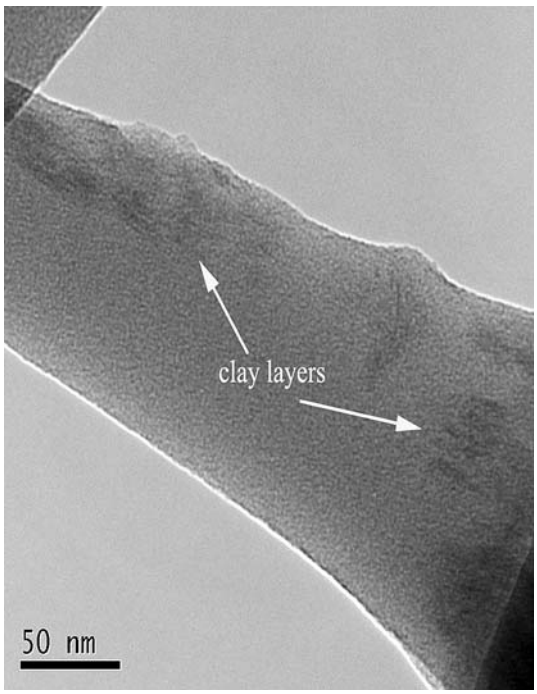

Fig. 4 HREM images of electrospun PA6 composite nanofiber with 4 wt.% Fe-OMT

distributed to form the fibrous web. It was observed that the electrospun nanofibers had variable fiber diameters. The morphology and average diameter of the electrospun PA6/Fe-OMT composite nanofibers were significantly affected by the amount of Fe-OMT added. The average diameters of the PA6 nanofibers were ranged from about several tens of nanometers to 100 nm. However, the average diameters of the PA6/Fe-OMT composite nanofibers were decreased compared to those of the pure PA6 nanofibers. The average diameter of electrospun PA6 composite nanofiber with 2 wt.% Fe-OMT was approximately 50 nm with an extremely homogeneous distribution and without any sign of bead formation, as indicated in Fig. 5b. When the amount of Fe-OMT increased to 4 wt.%, the average diameter of composite nanofibers was further decreased to several tens of nanometers. The addition of quaternary ammonium salts as an organic modifier increased the charge density in ejected jets, and thus stronger elongation forces were imposed to the jets because of the self-repulsion of the excess charges under the electrical field, resulting in substantially straighter shape and smaller diameter of electrospun fibers. Meanwhile, the conductivity of the PA6 solution was also another major factor affecting the morphology and diameter of the electrospun PA6 nanofibers. The loading Fe-OMT containing a quaternary ammonium ion ($C_{16}H_{33}(CH_3)_3N^+$) as an organic modifier and Na^+ and Zn^{2+} ions located between MMT layers improved the conductivity of PA6/Fe-OMT solutions [6, 10, 16–18]. As expected, the increase in the solution conductivity caused a

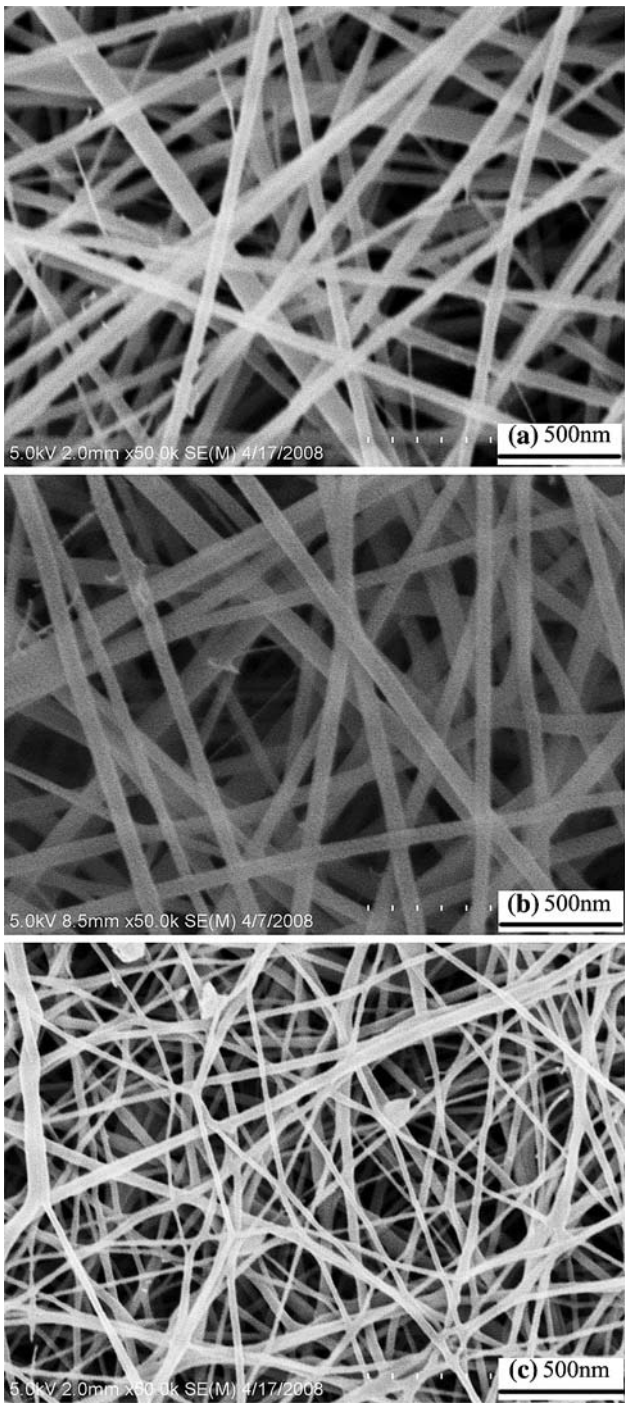

Fig. 5 SEM images of (**a**) PA6 nanofiber, (**b**) PA6/Fe-OMT2, and (**c**) PA6/Fe-OMT4 composite nanofibers

significant decrease in the average diameter of the PA6/Fe-OMT composite nanofibers.

Thermal stability

Thermal stability of the electrospun fibers was evaluated using TGA in nitrogen atmosphere. The TGA curves for

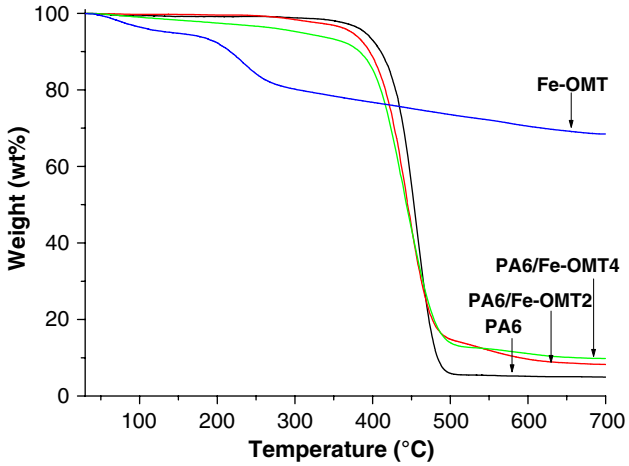

Fig. 6 TGA curves of Fe-OMT, electrospun PA6 nanofiber, and PA6/Fe-OMT composite nanofibers

Fe-OMT, pure PA6 nanofiber, and PA6/Fe-OMT composite nanofibers with different OMT loadings are shown in Fig. 6. It can be seen from the TGA curves that there were three-step degradation processes for Fe-OMT. The first step of degradation occurred roughly at the temperature lower than 150 °C, corresponding to the degradation of adsorbed water of silicate clay interlayers. The second step happened from about 150 to 300 °C. This step may be assigned to Hofmann elimination reaction of alkylammonium cations modified clays [3, 19]. The third step at about higher than 300 °C may be assigned to the structure-water loss process of the dehydroxy reaction within the silicate clay sheets and structure collapse of clay sheets [20, 21]. Under pyrolytic condition, PA6 nanofibers and PA6/Fe-OMT composite nanofibers degraded in one step. The onset thermal stability of the PA6/Fe-OMT composite nanofibers was not enhanced relative to that of pure PA6 nanofiber. The onset temperature of the degradation (5 wt.% weight loss) for the PA6/Fe-OMT composite nanofibers reduced from 390.3 °C for the pure PA6 nanofiber to 373.6 °C and 327.6 °C, respectively. The reasons may be that the alkylammonium cations were thermally instable and degraded in advance. Meanwhile, the alkylammonium cations in Fe-OMT could suffer decomposition following the Hofmann elimination reaction [3, 19], and its product would catalyze the degradation of PA6 materials. Thirdly, the clay itself could also catalyze the degradation of polymer materials [22]. These three aspects would reduce the thermal stability of PA6 composite nanofibers. However, the yield of charred residue at 700 °C for the PA6/Fe-OMT composite nanofibers was enhanced from 4.94% for the pure PA6 nanofiber to 8.23% and 9.78%, respectively. The reasons may be that the cations of some transition metals (e.g., Fe^{3+}) promoted the molecular cross-linking and increased the charred residue.

The effect was attributed to the ability of the cation to form complexes in which the metal atoms were coordinately bonded to the carbonyl oxygen atom of the amide group and are surrounded by polar solvent molecules [23]. It was also suggested that Fe^{3+} cations facilitated decomposition of hydroperoxides through a reversible oxidative-reductive catalytic process between Fe^{3+} and Fe^{2+} [12]. The Fe ion was also the operative site for radical trapping during the thermal degradation of the composite nanofibers [24]. The increased charred residue amount contributed to the improved thermal stability of the PA6 composite nanofibers. Besides, this was also attributed to the nano-size silicate clay layers which could presumably facilitate the reassembly of lamellas to form three-dimensional char, which might occur on the surface of the composite nanofibers and create a physical protective barrier. Meanwhile, the silicate clay layers could act as a superior insulator and mass-transport barrier and subsequently mitigate the escape of volatile products generated during the thermal decomposition [8, 25].

Crystalline properties

To study the effect of nanoclay on polymorphism in the electrospun nanofibers, wide-angle XRD measurements were conducted on both electrospun nanofibers of PA6 and PA6/Fe-OMT composites. The corresponding wide-angle XRD patterns are shown in Fig. 7. It is obvious that both electrospun PA6 nanofibers exhibited the characteristic peak at $2\theta = 21.3^{o}$ which was readily confirmed as the γ-form crystals of PA6. The corresponding d-spacing was 0.417 nm, associated with the (001) crystal planes. Compared to the pure PA6 nanofiber, the peak intensity of the γ-form crystals of PA6 had notable increases for the PA6/Fe-OMT composite nanofibers. It revealed that the PA6/Fe-OMT composite nanofibers contained greater amounts of the γ-crystal form than the PA6 nanofiber. The wide-angle XRD results suggested that electrospinning behaved in the same manner as high-speed melt-spinning, predominantly giving rise to the γ-form crystalline structure. Nanoclay played an important role in increasing the heterogeneous nucleation of the γ-form [2, 7, 26]. It can be also found from Fig. 7 that the weak diffraction peaks at 20.3^{o} and 23.3^{o} were associated with the α-phase of PA6 crystallites for the composite nanofibers [2, 26]. Even though a small amount of α-form crystals co-existed in the PA6/Fe-OMT composite nanofibers, the γ-crystals were predominantly formed. The results indicated that the presence of Fe-OMT induced the crystalline structure formation of α-form. The reasons may be that the crystal formation usually included two stages, which were nucleation and crystal growth. The nano-size clay platelets were effective nucleating agents and promoted the heterogeneous nucleation.

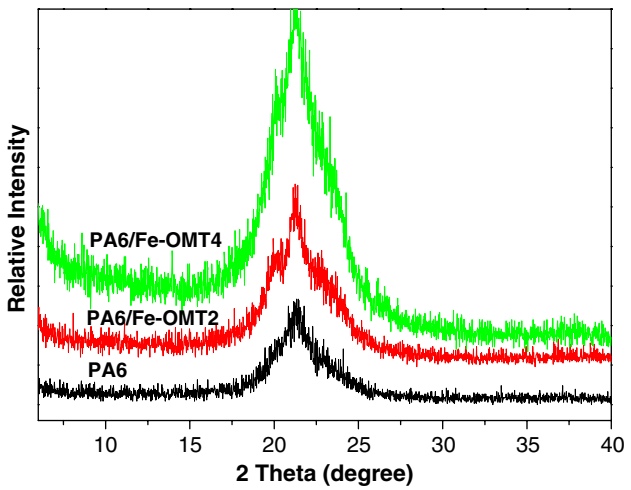

Fig. 7 Wide-angle XRD patterns of electrospun PA6 nanofiber and PA6/Fe-OMT composite nanofibers

Conclusions

In this article, Fe-montmorillonite was synthesized by hydrothermal method and then was modified by CTAB. The PA6/Fe-OMT composite nanofibers were successfully prepared by facile compounding and electrospinning. The structures, thermal stability, and crystalline properties of the electrospun composite nanofibers were investigated. The FTIR and EDX confirmed the presence of Fe-OMT in the composite nanofibers. The results from XRD and HREM indicated that the silicate clay layers were detected to exfoliate and align along the axis of the composite nanofibers. It was observed from SEM images that the loading of the Fe-OMT led to the decreases of nanofiber diameters, due to the increased conductivity of PA6 polymer solution. Compared to the PA6 nanofiber, the composite nanofibers showed improved thermal stability, attributed to the superior insulator, mass-transport, and physical protective barriers of silicate clay layers. The wide-angle XRD analyses revealed that the presence of nanoclays improved the γ-form crystals and induced the formations of α-form crystals of the PA6. The reasons may be that the silicate clay platelets were effective nucleating agents and promoted the heterogeneous nucleation of the PA6.

Acknowledgements The work was financially supported by the Program for New Century Excellent Talents in University (No. NCET-06-0485), the Specialized Research Fund for the Doctoral Program of Higher Education (No. 20060295005), Program for Innovative Team of Jiangnan University (PIRTJiangnan), and Program of Jiangnan University (No. 206000-21050737).

References

1. Shonaike GO, Advani SG (2003) Advanced polymeric materials: structure property relationships. C.R.C. Press, Boca Raton
2. Kim GM, Michler GH, Ania F, Balta Calleja FJ (2007) Polymer 48:4814. doi:10.1016/j.polymer.2007.05.082
3. Zhu J, Morgan AB, Lamelas FJ, Wilkie CA (2001) Chem Mater 13:3774. doi:10.1021/cm000984r
4. Vaia RA, Ishii H, Giannelis EP (1993) Chem Mater 5:1694. doi:10.1021/cm00036a004
5. Fong H, Liu WD, Wang CS, Vaia RA (2002) Polymer 43:775. doi:10.1016/S0032-3861(01)00665-6
6. Li L, Bellan LM, Craighead HG, Frey MW (2006) Polymer 47:6208. doi:10.1016/j.polymer.2006.06.049
7. Yoon KH, Polk MB, Min BG, Schiraldi DA (2004) Polym Int 53:2072. doi:10.1002/pi.1630
8. Wang M, Hsieh AJ, Rutledge GC (2005) Polymer 46:3407. doi:10.1016/j.polymer.2005.02.099
9. Ji Y, Li BQ, Ge SR, Sokolov JC, Rafailovich MH (2006) Langmuir 22:1321. doi:10.1021/la0525022
10. Hong JH, Jeong EH, Lee HS, Baik DH, Seo SW, Youk JH (2005) J Polym Sci Polym Phys 43:3171. doi:10.1002/polb.20610
11. Lee YH, Lee JH, An IG, Kim C, Lee DS, Lee YK et al (2005) Biomaterials 26:3165. doi:10.1016/j.biomaterials.2004.08.018
12. Liu J, Hu Y, Wang SF, Song L, Chen ZY, Fan WC (2004) Colloid Polym Sci 282:291. doi:10.1007/s00396-003-0978-y
13. Nagase T, Iwasaka T, Ebina T, Hayashi H, Onodera Y, Dutta NC (1999) Chem Lett 4:303. doi:10.1246/cl.1999.303
14. Kong QH, Hu Y, Lu HD, Chen ZY, Fan WC (2005) J Mater Sci 40:4505. doi:10.1007/s10853-005-0855-9
15. Chen GM, Shen DY, Feng M, Yang MS (2004) Macromol Rapid Commun 25:1121. doi:10.1002/marc.200400079
16. Zong XH, Kim K, Fang DF, Ran SF, Hsiao BS, Chu B (2002) Polymer 43:4403. doi:10.1016/S0032-3861(02)00275-6
17. Son WK, Youk JH, Lee TS, Park WH (2004) Polymer 45:2959. doi:10.1016/j.polymer.2004.03.006
18. Choi JS, Lee SW, Jeong L, Bae SH, Min BC, Youk JH et al (2004) Int J Biol Macromol 34:249. doi:10.1016/j.ijbiomac.2004.06.001
19. Xie W, Gao ZM, Pan WP, Vaia R, Hunter DL, Singh A (2000) Polym Mater Sci Eng 83:284
20. Xie W, Gao ZM, Pan WP, Hunter D, Singh A, Vaia R (2001) Chem Mater 13:2979. doi:10.1021/cm010305s
21. Xie W, Xie RC, Pan WP, Hunter D, Koene B, Tan LS et al (2002) Chem Mater 14:4837. doi:10.1021/cm020705v
22. Zhao CG, Qin HL, Gong FL, Feng M, Zhang SM, Yang MS (2005) Polym Degrad Stab 87:183. doi:10.1016/j.polymdegradstab.2004.08.005
23. Dunn P, Sansom GF (1969) J Appl Polym Sci 13:1657. doi:10.1002/app.1969.070130807
24. Zhu J, Uhl FM, Morgan AB, Wilkie CA (2001) Chem Mater 13:4649. doi:10.1021/cm010451y
25. Gilman JW, Jackson CL, Morgan AB, Harris R, Manias E, Giannelis EP (2000) Chem Mater 12:1866. doi:10.1021/cm0001760
26. Giza E, Ito H, Kikutani T, Okui N (2000) J Macromol Sci B 39:545. doi:10.1081/MB-100100403